



---

Applied Computational  
Electromagnetics Society


---



Newsletter  
Volume 12 - No. 1  
ISSN 1056-9170



March 1997



# Application of the Finite-Difference Time-Domain Method to Bioelectromagnetic Simulations

Cynthia M. Furse  
Department of Electrical Engineering  
University of Utah  
Salt Lake City, Utah 84112

## I. Introduction

The finite-difference time-domain (FDTD) method has been used extensively over the last decade for bioelectromagnetic dosimetry – numerical assessment of electromagnetic fields coupled to biological bodies [Gandhi, Lin & Gandhi]. Values of interest in these assessments include induced current or current density and specific absorption rate (SAR), which is a measure of absorbed power in the body. The FDTD algorithm is extremely simple and efficient, which has made it one of the most versatile numerical methods for bioelectromagnetic simulations. It is particularly well suited to these applications because it can efficiently model the heterogeneity of the human body with high resolution (often on the order of 1mm), can model anisotropy and frequency-dependent properties as needed, and can easily model a wide variety of sources coupled to the body. It has been used to analyze whole-body or partial-body exposures to spatially uniform (far field) or non-uniform (near-field) sources. These sources may be sinusoidally varying (continuous wave (CW)) or time-varying such as those from an electromagnetic pulse (EMP). The FDTD method has been used for applications over an extremely wide range of frequencies, from 60 Hz through 6 GHz, and also for broad-band applications. This paper describes several of these applications, and some of the details of how the FDTD method is applied to bioelectromagnetic simulations.

## II. The Finite-Difference Time-Domain Method

The FDTD method was originally developed by [Yee] and has been described extensively in the literature [Kunz & Luebbers; Taflove]. This method is a direct solution of the differential form of Faraday's and Ampere's laws

$$\nabla \times E = -\mu \frac{\partial H}{\partial t} \quad (1)$$

$$\nabla \times H = \sigma E + \epsilon \frac{\partial E}{\partial t} \quad (2)$$

Assuming that  $\epsilon$  and  $\mu$  are isotropic, frequency-independent, and constant over the region where the equation is being solved, (1) and (2) can be divided into six partial differential equations

$$\frac{\partial H_x}{\partial t} = \frac{-1}{\mu} \left( \frac{\partial E_z}{\partial y} - \frac{\partial E_y}{\partial z} \right) \quad (3a)$$

$$\frac{\partial H_y}{\partial t} = \frac{-1}{\mu} \left( \frac{\partial E_x}{\partial z} - \frac{\partial E_z}{\partial x} \right) \quad (3b)$$

$$\frac{\partial H_z}{\partial t} = \frac{-1}{\mu} \left( \frac{\partial E_y}{\partial x} - \frac{\partial E_x}{\partial y} \right) \quad (3c)$$

$$\frac{\partial E_x}{\partial t} = \frac{1}{\varepsilon} \left( \frac{\partial H_z}{\partial y} - \frac{\partial H_y}{\partial z} - \sigma E_x \right) \quad (4a)$$

$$\frac{\partial E_y}{\partial t} = \frac{1}{\varepsilon} \left( \frac{\partial H_x}{\partial z} - \frac{\partial H_z}{\partial x} - \sigma E_y \right) \quad (4b)$$

$$\frac{\partial E_z}{\partial t} = \frac{1}{\varepsilon} \left( \frac{\partial H_y}{\partial x} - \frac{\partial H_x}{\partial y} - \sigma E_z \right) \quad (4c)$$

The model space is then divided into a lattice of discrete unit cells, which is shown in Figure 1. A space point in the lattice is defined as  $(x,y,z) = (i\Delta x, j\Delta y, k\Delta z)$ , and any function of space and time is defined as  $F^n(i,j,k) = F(i\Delta x, j\Delta y, k\Delta z, n\Delta t)$  where  $\Delta x, \Delta y, \Delta z$  are the lattice space resolutions in the  $x,y,z$  coordinate directions,  $\Delta t$  is the time increment, and  $i,j,k$  and  $n$  are integers.

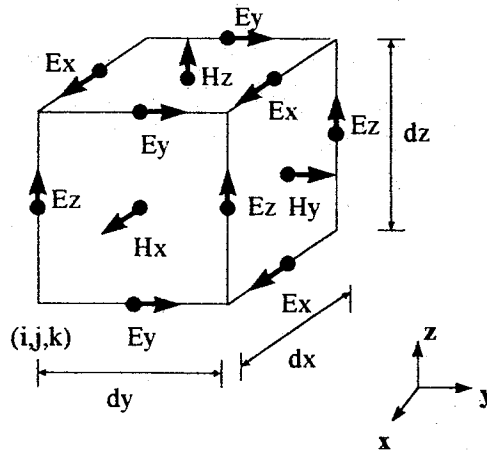


Figure 1: The "Yee" cell or FDTD lattice showing distribution of the electric and magnetic field components

The differential equations in (3) and (4) are then converted into difference equations using the central difference approximations

$$\frac{\partial F^n(i,j,k)}{\partial x} = \frac{F^n(i + \frac{1}{2}, j, k) - F^n(i - \frac{1}{2}, j, k)}{\Delta x} \quad (5a)$$

and

$$\frac{\partial F^n(i,j,k)}{\partial t} = \frac{F^{n+\frac{1}{2}}(i,j,k) - F^{n-\frac{1}{2}}(i,j,k)}{\Delta t} \quad (5b)$$

For evenly spaced lattices, the error for these equations is  $(\Delta x)^2$  and  $(\Delta t)^2$ , respectively. Thus, these first order difference equations provide second order accuracy. Since the field components are interleaved on each unit cell as shown in Figure 1, the E and H components are half a cell apart, which is referred to as a "leap-frog" scheme. In addition to being leap-frogged in space, they are also leap-frogged in time. The E field is assumed to be at time  $n\Delta t$ , and the H field is assumed to be at time  $(n+1/2)\Delta t$ .

Applying the central difference approximations in (5a) and (5b) to (3a) and (4a) gives the difference equations

$$H_x^{n+1/2}(i, j, k) = H_x^{n-1/2}(i, j, k) + Chy(i, j, k)[E_x^n(i, j, k) - E_x^n(i, j+1, k)] + Chz(i, j, k)[E_y^n(i, j, k+1) - E_y^n(i, j, k)] \quad (6)$$

and

$$E_x^{n+1}(i, j, k) = (CE)E_x^n(i, j, k) + Cey(i, j, k)[H_x^{n+1/2}(i, j, k) - H_x^{n+1/2}(i, j-1, k)] + Cez(i, j, k)[H_y^{n+1/2}(i, j, k) - H_y^{n+1/2}(i, j, k-1)] \quad (7)$$

In these equations, E and H are generally of different orders of magnitude. To reduce the numerical errors which arise from taking the divided differences of significantly different values, a normalization factor,

$$H(\text{programmed}) = \sqrt{\mu_o / \epsilon_o} H(\text{physical}) \quad (8)$$

is used to make E and H be of the same order of magnitude. Using the value  $\Delta t = \Delta x / (2c_o)$ , the constants in equations (6) and (7) become

$$\begin{aligned} Chy &= c_o \Delta t / (u_r(i, j, k) \Delta y) \\ Chz &= c_o \Delta t / (u_r(i, j, k) \Delta z) \\ CE &= \frac{2\epsilon_o \epsilon_r(i, j, k) - \Delta t \sigma(i, j, k)}{2\epsilon_o \epsilon_r(i, j, k) + \Delta t \sigma(i, j, k)} \\ Cey &= \frac{2\Delta t \sqrt{\epsilon_o / \mu_o}}{\Delta y (2\epsilon_o \epsilon_r(i, j, k) + \Delta t \sigma(i, j, k))} \\ Cez &= \frac{2\Delta t \sqrt{\epsilon_o / \mu_o}}{\Delta z (2\epsilon_o \epsilon_r(i, j, k) + \Delta t \sigma(i, j, k))} \end{aligned} \quad (9)$$

Similar equations and constants are obtained for (3b), (3c), (4b), (4c). These constants can be used to represent anisotropic properties which are present in muscle and cardiac tissues at low frequencies by allowing the values of  $\epsilon_r, \sigma, \mu_r$  to be different in the x, y, z directions. For biological tissues,  $\mu_r = 1$ .

The steps in the FDTD solution are:

- 1) Define model values of  $\epsilon_r, \sigma, \mu_r$  at each location i, j, k, and calculate the constants given in (9).
- 2) Assume initial conditions (usually that all fields and the source are zero).

- 3) For each time step,  $n$ 
  - a) Specify fields at source.
  - b) Calculate  $E^n$  for all locations.
  - c) Calculate  $H^{n+1/2}$  for all locations.
- 4) Stop when the solution has converged. For transient fields, this means all of the fields have died away to zero. For sinusoidal fields, this means that all of the fields have converged to a steady-state sinusoidal value.

There are two constraints controlling what values are defined for the space resolutions,  $\Delta x$ ,  $\Delta y$ ,  $\Delta z$ , and the time resolution,  $\Delta t$ . The space resolution in bioelectromagnetic simulations is generally controlled by the grid resolution of the human model. Since these models are extremely difficult to create, only a few models are available in the world, and while grids can be adjusted somewhat (cells combined to reduce resolution, or subdivided to increase the resolution), for the most part only an isolated set of resolutions are available. Resampling of the model is possible, but in general, the grid resolution is more or less set. What is important is to determine the maximum frequency which a given resolution can be accurately used for. A rule of thumb is that the largest grid dimension,  $\Delta x$ , for instance, should not be larger than  $\lambda/10$ , where  $\lambda$  is the smallest wavelength in the model. This limitation comes from the fact that the numerical grid produces a certain amount of artificial (numerical) dispersion which increases with the grid size and direction of propagation as shown in Figure 2. When the resolution is  $\lambda/10$ , the numerical dispersion is approximately 1%.

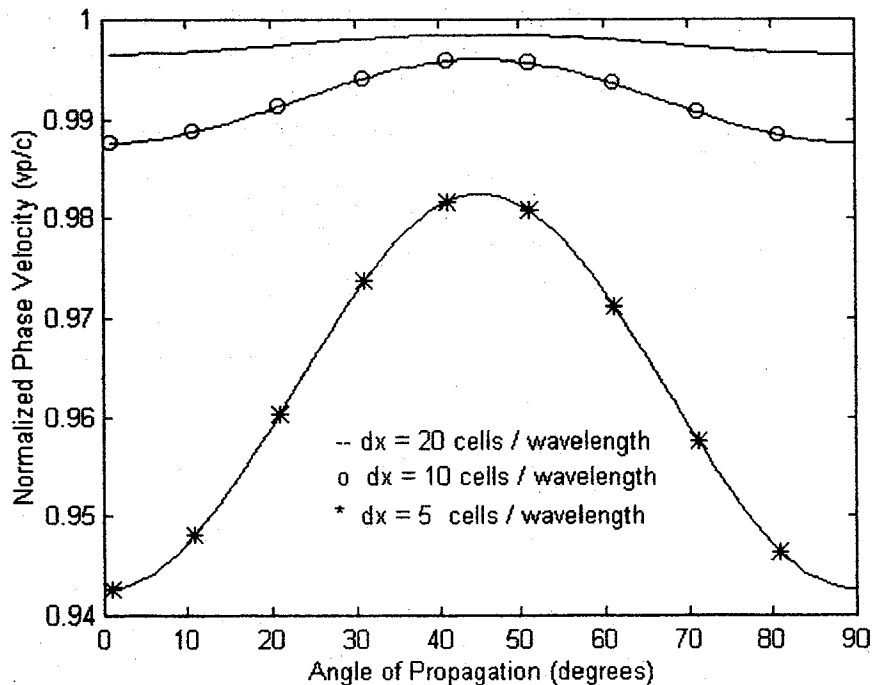


Figure 2: Variation of the numerical phase velocity with wave propagation angle in two-dimensional FDTD grid for three dimensions [Taflove]

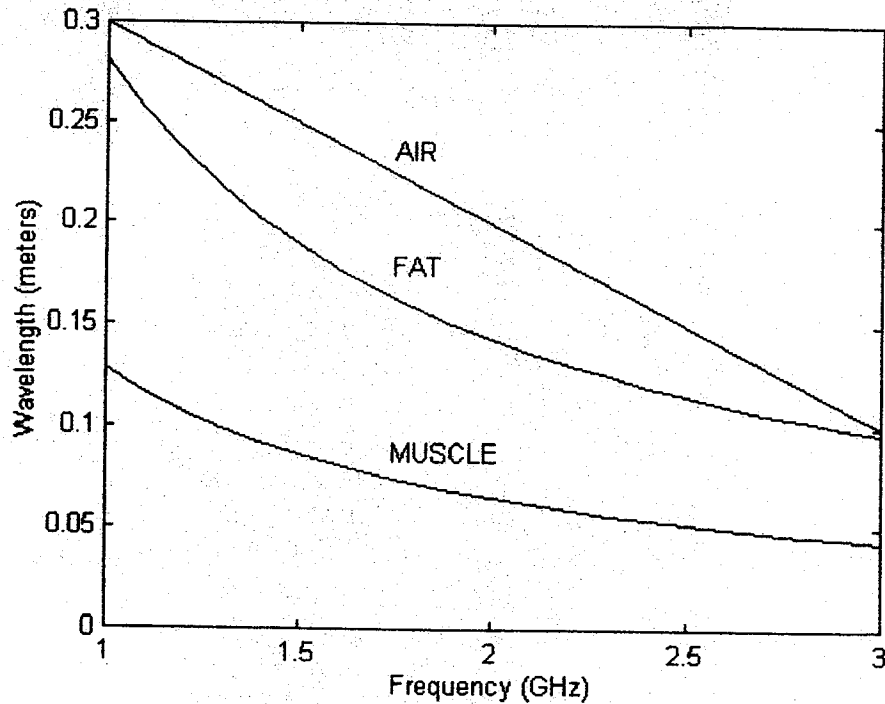


Figure 3: Wavelength of muscle, fat, and air as a function of frequency. Additional body tissues fall between fat and muscle.

In order to determine the maximum frequency a given grid size is suitable for, Figure 3 shows the wavelength as a function of frequency for several tissues of the body. Not only does the standard relationship between electrical properties and frequency control the wavelength, but the electrical properties of the tissues also vary with frequency. Although it is ideal to limit the use of a given grid to frequencies which make the resolution be less than  $\lambda/10$ , bioelectromagnetic simulations sometimes push this limit, and resolutions of  $\lambda/4$  have been successfully used [Furse, et al., 1994]. For many simulations, this does not cause problems, because the wave is absorbed before it can propagate far, so the dispersion error is relatively small.

A second constraint is that to maintain the stability of the FDTD simulation the time resolution must be sufficiently small such that

$$\Delta t \leq \frac{1}{v_{\max} \sqrt{\frac{1}{\Delta x^2} + \frac{1}{\Delta y^2} + \frac{1}{\Delta z^2}}} \quad (10)$$

where  $v_{\max}$  is the maximum velocity of propagation in any material in the model. The value of  $\Delta t = \Delta x/(2c_0)$ , which is used in many FDTD codes, is well within this limit. These two constraints provide limits on the time and space resolutions which must be used in order to accurately model time domain behavior of a given waveform.

But what happens when a waveform is used which has frequency components above the "limit" of the FDTD grid, such as in many pulsed simulations? In this case, the

numerical dispersion in FDTD solutions serves an interesting purpose. It disperses these high frequency components, thus making it impossible for them to propagate and cause frequency aliasing errors [Furse, 1994]. This makes it possible to use any waveform, even a narrow rectangular pulse with near-infinite frequency spectrum as a source for FDTD simulations. The high frequency components do not propagate, so are effectively filtered out of both the time and frequency domain simulations. They provide no information, but also do not cause any errors.

### III. The Frequency-Dependent FDTD Method

The electrical properties of biological tissues vary significantly with frequency, as shown in Figure 4. For single-frequency simulations, the FDTD method can be used, with the particular tissue properties at that frequency, but for broad-band simulations, this is not sufficient. The frequency-dependent finite-difference time-domain (FD)<sup>2</sup>TD method is therefore used to overcome this limitation. Two general approaches to the (FD)<sup>2</sup>TD method have been developed. One approach is to convert the complex permittivity from the frequency domain to the time domain and convolve this with the time-domain electric fields to obtain time-domain fields for dispersive materials. This discrete time-domain convolution may be updated recursively for some rational forms of complex permittivity, which removes the need to store the time history of the fields and makes the method feasible. This method has been applied to materials described by first-order Debye relaxation equation [Luebbers, et al. 1990; Bui et al.; Sullivan 1992], a second-order Lorentz equation with multiple poles [Luebbers, et al., 1992], and to a gaseous plasma [Luebbers, et al., 1991].

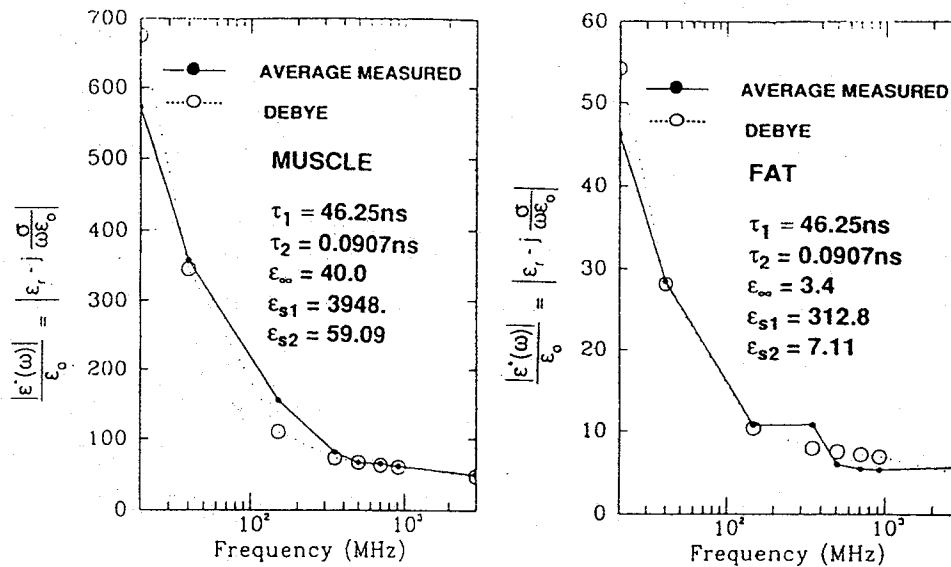


Figure 4: Electrical properties of fat and muscle as a function of frequency. Measured values from the literature are compared to those modeled with a second-order Debye equation [Furse, et al., 1994]

A second approach is to add a differential equation relating the electric flux density  $\mathbf{D}$  to the electric field  $\mathbf{E}$  and to solve this new equation simultaneously with the standard FDTD equations. This method has been applied to one-dimensional and two-dimensional examples with materials described by a first-order Debye equation or second-order single-pole Lorentz equations [Joseph, et al.; Lee, et al.], to 3D sphere and homogeneous two-thirds muscle equivalent man model with properties described by a second-order Debye equation [Gandhi, et al., 1993a, 1993b; Furse, et al., 1994], and to a heterogeneous model of the human body exposed to ultra-wide band electromagnetic pulses [Gandhi and Furse, 1993], as described below.

The time-dependent Maxwell's equations have already been given in (1) and (2). Ampere's law can be rewritten as

$$\nabla \times H = \frac{\partial D}{dt} \quad (11)$$

where the flux density vector  $\mathbf{D}$  is related to the electric field  $\mathbf{E}$  through the complex permittivity  $\epsilon^*(\omega)$  of the local tissue by the following equation:

$$\mathbf{D} = \epsilon^*(\omega) \mathbf{E} \quad (12)$$

Since (1) and (11) are to be solved iteratively in the time domain, (12) must also be expressed in the time domain. This may be done by choosing a rational function for  $\epsilon^*(\omega)$  such as the Debye equation with two relaxation constants:

$$\epsilon^*(\omega) = \epsilon_o \left[ \epsilon_\infty + \frac{\epsilon_{s1} - \epsilon_\infty}{1 + j\omega\tau_1} + \frac{\epsilon_{s2} - \epsilon_\infty}{1 + j\omega\tau_2} \right] \quad (13)$$

Rearranging (13) and substituting in (12) gives

$$D(\omega) = \epsilon^*(\omega)E(\omega) = \epsilon_o \frac{\epsilon_s + j\omega(\epsilon_{s1}\tau_2 + \epsilon_{s2}\tau_1) - \omega^2\tau_1\tau_2\epsilon_\infty}{1 + j\omega(\tau_1 + \tau_2) - \omega^2\tau_1\tau_2} E(\omega) \quad (14)$$

where the dc (zero frequency) dielectric constant is given by  $\epsilon_s = \epsilon_{s1} + \epsilon_{s2} - \epsilon_\infty$ .

Assuming  $e^{j\omega t}$  time dependence, (14) can be written as a time-domain differential equation

$$\tau_1\tau_2 \frac{\partial^2 D}{\partial t^2} + (\tau_1 + \tau_2) \frac{\partial D}{\partial t} + D = \epsilon_o \left[ \epsilon_s E + (\epsilon_{s1}\tau_2 + \epsilon_{s2}\tau_1) \frac{\partial E}{\partial t} + \epsilon_\infty\tau_1\tau_2 \frac{\partial^2 E}{\partial t^2} \right] \quad (15)$$

As in [Gandhi, et al., 1993a, 1993b], this equation is then converted into a second order difference equation, which requires storage of one past time step for the  $\mathbf{D}$  and  $\mathbf{E}$  fields. Equations (1) and (11) are then solved subject to (15). The steps for the (FD)<sup>2</sup>TD method are:



- 1) Define value of  $\epsilon^*(\omega)$  for each tissue and use least-squares to find an optimal fit of  $\epsilon_{s1}, \epsilon_{s2}, \epsilon_{\infty}, \tau_1, \tau_2$  in (13) for each tissue. Calculate constants for (15).
- 2) Assume initial conditions (usually that all fields and the source are zero).
- 3) For each time step,  $n$ 
  - a) Specify fields at source.
  - b) Calculate  $\mathbf{E}^n$  for all locations.
  - c) Calculate  $\mathbf{D}^n$  for all locations.
  - d) Calculate  $\mathbf{H}^{n+1/2}$  for all locations.
- 4) Stop when the solution has converged. For transient fields, this means all of the fields have died away to zero. Continuous wave fields are not used in  $(\text{FD})^2\text{TD}$  simulations (since they are not broad-band, FDTD is used).

#### IV. Methods of converting from Time to Frequency Domain

Since the FDTD and  $(\text{FD})^2\text{TD}$  methods are intrinsically time-domain methods, when frequency-domain information is required, some method of conversion must be used. Examples of frequency-domain parameters which are calculated are magnitudes of fields (for one or more frequencies), specific absorption rate (SAR), which is calculated from field magnitudes, currents or current densities, and integrated properties such as radiation pattern or total power absorbed or reflected. There are several methods which have historically been used to transfer from sampled time domain to frequency domain data for bioelectromagnetic applications. These are peak detection methods, Fourier transform methods, and a direct calculation method. The goal of all of these methods is to detect the magnitudes and possibly the phases of the time-domain fields. Which of the methods is used is particularly important in bioelectromagnetic simulations, since it is common for a huge number of time-to-frequency domain conversions to be required (such as at every location in the body for calculation of SAR or current density distributions), and the computer time and memory can be nearly as large as those required for the time-domain simulation itself.

The peak detection method is of historical interest only, as it is the least efficient and least accurate of the methods. The values of successive time steps in a sinusoidal simulation are compared to determine when the peak of the wave has been reached, and this value is recorded as the magnitude of the wave. This method is time-consuming (a series of IF-THEN computer statements), and requires storage of past-time values for comparison. It is the least accurate of the methods, as the peak may occur between successive time samples, so the value recorded for magnitude will be slightly lower than the actual magnitude. Phase calculations using this method are highly inaccurate for this reason.

The Fourier transform method is probably the most widely used of the methods of determining magnitude and phase, and is highly accurate. For either transient or sinusoidal calculations, the complex magnitude of the wave can be calculated from the time-domain waveform using

$$G(k\Delta f) = \Delta t \sum_{n=0}^N g(n\Delta t) e^{-j \frac{2\pi k n \Delta t}{N}} \quad (16)$$

where

$G(k\Delta f)$  is the complex magnitude

$g(n\Delta t)$  is the time-domain waveform

$\Delta f$  is the frequency resolution

$\Delta t$  is the time resolution

$n$  is the time step index = 0, 1, 2, ... N

$k$  is the frequency index

$N$  is the length of the Fourier transform =  $1/(\Delta f \Delta t)$

For transient simulations, the simulation may converge, and all field values,  $g(n\Delta t)$  may go to zero before the summation in (16) is complete. In that case, the summation can be stopped before  $N$  summations, which saves computational time. For sinusoidal (single-frequency) applications, the summation is done for one cycle after the simulation has converged to steady-state. This requires running the FDTD simulation an additional cycle, which can be burdensome or even impossible at lower frequencies.

The Fourier transform in (16) can be calculated with either the Fast Fourier Transform (FFT) or the discrete Fourier transform (DFT) in (16). It has been shown [Furse and Gandhi, 1995] that the DFT is actually faster than the FFT for FDTD applications, although many people still use the FFT method because of the convenience of prepackaged Fourier transform software. Both methods are equally accurate.

Time decimation [Bi, et al.] can be used to significantly reduce the length of the sum in (16), and improve the computational efficiency of the algorithm. This method recognizes that, although the FDTD constraints that  $\Delta x \leq \lambda/10$  and  $\Delta t = \Delta x/(2c_0)$  produce a sampled time sequence from the simulation which is far over-sampled in terms of the Nyquist criterion, that only two samples per cycle are actually required for accurate calculation of the magnitude and phase of the wave. Thus, the number of samples used in the Fourier transform can be significantly reduced. This applies to both transient and steady-state simulations.

Taking this one step further, a direct method [Furse] for finding magnitude and phase provides great flexibility of magnitude and phase calculations coupled with efficiency and accuracy. It is apparent that for sinusoidal simulations the two samples which are used need not be evenly spaced. This method is based on writing two equations in two unknowns (magnitude and phase) for the time-domain fields, and then solving the directly for the magnitude and phase. At a given location in space, we can write

$$\begin{aligned} A \sin(\omega t_1 + \phi) &= g_1 \\ A \sin(\omega t_2 + \phi) &= g_2 \end{aligned} \quad (17)$$

where  $A$  is the magnitude,  $\phi$  is the phase, and  $\omega (=2\pi F)$  is the angular frequency. At two times,  $t_1$  and  $t_2$ , the two values of  $g_1$  and  $g_2$  are known from the FDTD simulation. Therefore, these two equations can be solved directly for the unknowns  $A$  and  $\phi$ . No theoretical constraints are given on  $t_1$  and  $t_2$ , so they can be taken to be the last two time steps of the simulation. This allows calculation of magnitude and phase with no additional computer memory, which is a considerable advantage in the large-scale simulations typical of bioelectromagnetic simulations. This method is also considerably more efficient than the Fourier transform methods, as it does not require a summation to be done over several (or several hundred) time steps. The DFT and peak detection methods require approximately as much computational time and memory as the FDTD simulation, if time-to-frequency domain conversions are required in all cells in the body, which is typical of bioelectromagnetic simulations. The direct method, on the other hand, requires virtually no computational time, and can be programmed with virtually no memory requirement. These significant advantages make it the primary method of choice for bioelectromagnetic simulations.

The direct solution method does have some limitations. First, it can only be used for single-frequency FDTD simulations. Second, it is only accurate when the simulation produces a clean, perfectly converged sine wave without DC offsets or noise.

The significant advantages of this method have led to its use in some novel applications. The first is the use of the direct method for determining convergence of sinusoidal simulations. It is relatively easy to tell when transient simulations have converged ... all the fields have gone to "zero". For sinusoidal simulations, this has been more difficult. Calculating the magnitude and phase historically required a full cycle of the simulation to be run "past convergence", and running still more cycles to check on convergence is often prohibitively expensive. Generally a few indicative test cases would be checked for convergence, and then similar simulations would be assumed to be converged in a similar amount of time. This direct method provides a way to calculate magnitude and phase with great efficiency, and without requiring a large number of time steps of the simulation to be run, so the calculations of magnitude and phase can be repeated within the simulation itself to test for convergence.

A second advance which this direct solution method has enabled is calculation of extremely low frequencies using the FDTD method. There has been no intrinsic limitation of the FDTD method for running low frequency simulations, but there was no method of extracting the magnitude and phase from these simulations. For a 6mm human model at 60 Hz, for instance, one cycle requires  $1.6 \times 10^9$  time steps. It is not feasible to run even an appreciable portion of a cycle, which would be required by the Fourier transform or peak detection methods. Using this direct method, the solution can be found with about 2000 time steps. This application presents some unique numerical challenges, as the fields change so little from one time step to another. Unlike higher-frequency simulations where round-off errors between two immediate time steps are negligible, significant numerical error is observed when calculating the magnitude and phase if the last two time steps are used for extremely low frequencies. For the simulation described in section VIII.A,  $t_1$

was taken to be 100 time steps before the final time step,  $t_2$ , which reduced the numerical errors in this calculation.

## V. Human Models and Tissue Properties

Model development is one of the significant challenges of numerical bioelectromagnetics. Models have progressed from the prolate spheroidal models of the human used during the 1970s to roughly 1cm models based on anatomical cross sections used during the 1980s [Gandhi, et al. 1992a ] to a new class of millimeter-resolution MRI-based models of the body which are the hallmarks of research in the 1990s [Gandhi and Furse, 1995; Dimbylow, 1995; Olley & Excell, 1995; Stuchly, et al., 1995]. MRI scans provide an ideal initial data base for voxel-based models of this type, but the scans alone do not define the types of tissue which are in each location. Instead, MRI scans provide a voxel map of MRI densities, which unfortunately do not have a one-to-one correspondence to tissue type. These images are interpreted as grey-scale images by which the several tissues can be "seen". Image segmentation is necessary to convert these density mappings into mappings of tissue type. This is generally done semi-manually, although automatic methods are under development.

Several MRI-based models of the human body [Gandhi and Furse, 1995; Dimbylow, 1995 ] or the head alone [Olley & Excell, 1995; Stuchly, et al., 1995; Jensen & Rahmat-Samii] are now in existence. With the exception of some basic automatic tissue classification based on MRI densities (dry tissue can be separated from wet tissue, for instance), these models have required significant effort to obtain, and there are many unique challenges in developing models suitable for use in bioelectromagnetic modeling.

First, there are issues which must be addressed in obtaining the MRI scans. It is important to use MR settings to optimize the contrast between the soft tissues, and to use saturation pulses to reduce pulsatile blood flow artifacts, and time gating to reduce blurring from breathing and the beating heart. Depending on the amount of time gating and optimization, scanning the complete body with a vertical resolution of 3mm takes 6 to 24 hours. The person being scanned will need to be repositioned during this time, as that is too long to expect a live person to hold still, and this presents some difficulties in rematching the images from successive positions. It is useful to position the person in exactly the stature that is desired for modeling, such as ensuring that the feet are in a "standing" position, as opposed to "relaxed", and that the head is in alignment with the spine, as opposed to on a pillow. Arms have caused significant difficulty in several modeling efforts, as in a relaxed position, they tend to fall out of the range of MRI scanning. Most of these problems are eliminated if a cadaver is used as the subject to be scanned, such as in the Visible Man project [National Library of Medicine], although the difficulty of positioning the model is still a problem, and this model [National Library of Medicine] is also missing portions of the arms due to limitations of scanning range. Using a cadaver provides challenges in itself, as body fluids tend to pool at the back of the body, organs shrink or swell, and airways collapse very soon after death. It has also been

observed that the overall height of the body increases by several cm when it is lying (such as in an MR machine) as opposed to standing, for both live humans and cadavers.

An additional problem with MR scanned images is there is a tradeoff between signal-to-noise ratio and a shift which is seen between fat and water-based tissues such as muscle. When the signal-to-noise ratio is optimized, the fat will appear slightly shifted in location relative to muscle. The shift may be as much as 4-5 mm [Gandhi & Furse, 1995]. In general this is a minor issue, as the majority of fat deposits are sufficiently large that this shift is inconsequential. While the fat shift may not cause much difficulty in defining the regions of fat, it does cause difficulty in defining the regions of skin. On the "read" side of the model, the fat obliterates the skin layer, making it appear very thin, while on the other side of the model, the skin appears very thick. A solution to this problem is to specify a pre-defined thickness of skin covering the whole body, and to apply this with a computer algorithm after image segmentation of the other tissues. This algorithm can be progressively refined as needed, to control the thickness of skin throughout different regions of the body.

An additional consideration when developing a model for bioelectromagnetic simulations is the question of uniqueness of individuals. It has been shown that the height of a person affects how much current will be induced by high voltage lines [Deno], and that the size of the head (children as compared to adults) affects the 1-gram averaged SAR from cellular telephones [Gandhi, et al., 1996]. It has also been shown that minimal differences in 1-gram averaged SARs from cellular telephones were obtained for several head models without the ear [Hombach, et al.], although it is likely that differences in ear shape could affect the 1-gram averaged SAR. The "average" man is defined in [Snyder, et al.]. Although it is unlikely that any given model which is scanned will provide exactly the same height, weight, and organ sizes of the reference man, this source is useful to compare given organ weights of a tissue segmented model to be certain they are similar to expected values. Another option is scaling the voxel size of the image-segmented model to obtain a model with exactly the height (176 cm) and weight (71 kg) of the reference man [Snyder, et al.].

As an example of one tissue segmented model, the MRI-based man model developed at the University of Utah was taken with an MRI voxel size of 1.875 x 1.875 x 3mm. The software ANALYZE, developed at the Mayo Clinic was used to segment the tissues. This package allows the user to define regions based on ranges of density, and convert each region into a tissue type. Proceeding to subsequent layers the density range is repeated, so that large, well-defined organs or bone can be readily defined. This somewhat automated the process of converting from density to tissue type, but it was still a tedious process, requiring a trained anatomist. The height of the volunteer was 176.4 cm, which is quite close to the height of 176 cm of the average "reference" man [Snyder, et al.], so no scaling was done in the vertical direction. The weight of the volunteer was 64 kg, which was somewhat lower than the average weight of 71 kg [Snyder, et al.], so the horizontal voxels were scaled to 1.974 mm, in order to bring the weight of the segmented model to 70.93 kg.

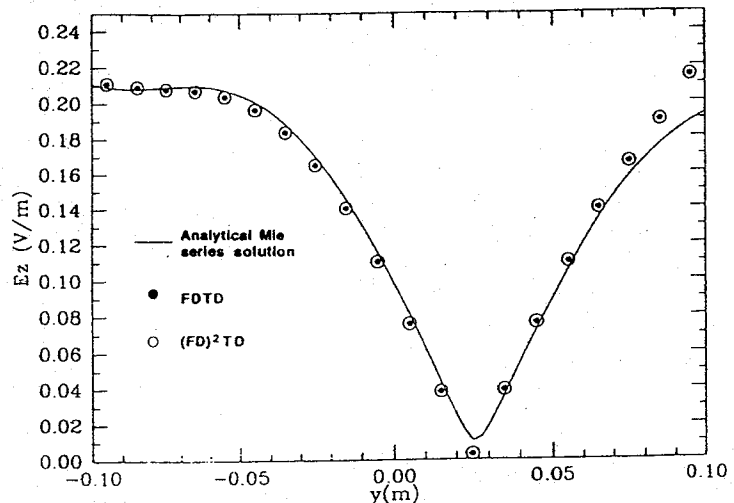
Once a tissue-segmented model has been developed, the electrical properties of the tissues are defined. The properties of human tissue change significantly with frequency, so it is essential to use data accurately measured at the frequency of interest. There is a wide range of published data on measured tissue properties [Gabriel; Stuchly & Stuchly; Rush, et al.; Durney, et al.; Geddes & Baker; Foster & Schwan], and work is still underway to measure and verify these properties. The most complete measurements have been done by [Gabriel], and these measurements are being tested for repeatability by other groups [Davis]. In addition to the measured values at individual frequencies from 10 Hz through 20 GHz for 30 tissue types, the data in [Gabriel] were fit to a 4<sup>th</sup> order Cole-Cole equation, which provides a good interpolation for electrical properties of tissues at any specific frequency of interest. This Cole-Cole interpolation is assumed to be a good interpolation above 1 MHz, where the data is well-defined in the literature, and should be used with caution in the region below 1 MHz, where literature is still sparse.

As expected, the results from bioelectromagnetic simulations are significantly affected by the electrical properties of the tissues which are used [Gandhi, et al., 1996], so it is important to use properties measured as accurately as possible.

## VI. Validation

The accuracy of the FDTD method has been extensively validated by comparing simulated results with analytical and measured results for sources in the far field coupled to a variety of geometries including square [Umashankar & Taflove] and circular [Umashankar & Taflove; Furse, et al., 1990; Taflove & Brodwin; Borup, et al.] cylinders, spheres [Holland, et al.; Gandhi & Chen, 1992; Sullivan, 1987; Gao & Gandhi], plates [Taflove, et al., 1985], layered half spaces [Oristaglio & Hohmann], and complicated geometries such as airplanes [Kunz & Lee]. Figure 5 shows the comparison for the electric fields calculated inside a 20-cm diameter sphere made up of 2/3 muscle irradiated by a plane wave at 200 MHz. The FDTD calculations are compared to the analytical solution based on the Bessel function expansion.

Figure 5: Magnitude of  $E_z$  along the y-axis of a 2/3 muscle sphere at 200 MHz. The plane-wave is incident from the y-direction. [Furse, et al., 1994]



In addition to these far-field validations, several near-field validations have also demonstrated that the FDTD method can be used to accurately model localized sources very near the human body. [Furse and Gandhi] One such example is the modeling a Hertzian (infinitesimal) dipole at 900 MHz located 1.5 cm from a 20-cm diameter brain-equivalent ( $\epsilon_r=43.0$ ,  $\sigma = 0.83$  S/m) sphere. This is a very near-field simulation of a curved (spherical) model. The infinitesimal dipole is modeled as a single Ez source location, and is excited with a ramped sinusoidal source where

$$E_z(\text{feedpoint}) = [1 - \cos(\omega t)] \sin(\omega t) \quad \text{for } 0 \leq t \leq T$$

$$= \sin(\omega t) \quad \text{for } t \geq T$$

where T is the period of the sine wave. This ramped sine wave has been shown to reduce high-frequency transients [Beuchler, et al.] and DC offsets [Furse, 1994] sometimes associated with unramped sine waves. The cubical cell size is  $\Delta = 5$  mm, which makes the sphere 40 cells in diameter. Figure 6 [Furse, et al., 1996] shows the relative SAR along the y-axis from the front edge of the sphere calculated using the FDTD method and compared to an analytical solution based on the Bessel function expansion [Dhondt & Martens].

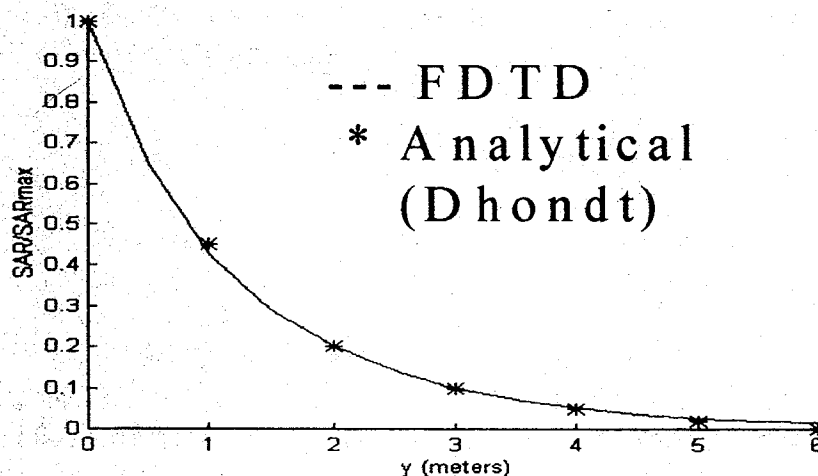


Figure 6: Relative SAR distribution along the y-axis of a homogeneous brain-equivalent sphere excited by an infinitesimal dipole. Analytical solution from [Dhondt and Martens]. FDTD from [Furse and Gandhi, 1996]

## VII. Calculation of SAR, currents, and 1-gram SAR, and temperature

The FDTD method calculates the time-domain vector **E** and **H** fields at every location inside and outside of the body. These can be converted to frequency domain fields (magnitude and phase at given frequencies) using the methods described in section IV. Values commonly of interest in bioelectromagnetic simulations are specific absorption rate, current density, total power absorbed, temperature rise, etc.

Specific absorption rate (SAR) at a given location is given by:

$$SAR(i, j, k) = \frac{\sigma(i, j, k)|E|^2}{2\rho(i, j, k)} \quad (18)$$

where  $\sigma(i,j,k)$  is the electrical conductivity and  $\rho(i,j,k)$  is the mass density at the location of interest.  $|E|^2$  is the magnitude of the electric field at the location of interest. Since the  $E_x, E_y, E_z$  components of this field are offset throughout the cell as shown in Figure 1, this requires that they be averaged to obtain the  $|E|$  at exactly the location of interest. For instance, if the SAR is desired at the bottom left corner of the cell,  $|E|$  is computed thus:

$$\begin{aligned} E_x(\text{corner}) &= [ E_x(i,j,k) + E_x(i-1,j,k) ] / 2. \\ E_y(\text{corner}) &= [ E_y(i,j,k) + E_y(i,j-1,k) ] / 2. \\ E_z(\text{corner}) &= [ E_z(i,j,k) + E_z(i,j,k-1) ] / 2. \\ |E|^2 &= E_x(\text{corner})^2 + E_y(\text{corner})^2 + E_z(\text{corner})^2 \end{aligned}$$

The 2 in the denominator of (18) converts the magnitudes of  $|E|$  calculated from FDTD from peak values to RMS. This precision in calculating  $|E|$  at a particular location in the cell is of minimal importance in far-field applications where the fields are not changing too rapidly within the cell. In near-field applications, such as analysis of cellular telephones, however, this is significant, as the fields are varying rapidly with the cells.

For near-field applications, such as cellular-telephones, numerical simulation is often used to determine if these devices comply with the ANSI/IEEE safety guidelines [ANSI] and newly-mandated FCC guidelines [FCC] which state that an exposure can be considered to be acceptable if it can be shown that it produces SAR's "below 0.08 W/kg, as averaged over the whole body, and spatial peak SAR values not exceeding 1.6 W/kg, as averaged over any 1 g of tissue (defined as a tissue volume in the shape of a cube)" [ANSI]. Because of the irregular shape of the body (eg. the ears) and tissue heterogeneities, a tissue volume in the shape of a cube of say, 1x1x1 cm will have a weight that may be in excess of, equal to, or less than 1 gram. Larger or smaller volumes in the shape of a cube may, therefore, need to be considered to obtain a weight of about 1 gram. Furthermore, for an anatomic model with parallelepiped voxels (such as the 1.974 x 1.974 x 3mm voxels of the University of Utah model), it is not very convenient to obtain exact cubical volumes even though nearly cubic shapes may be considered. It is therefore desirable to take volumes as close to cubical as possible (such as 5x5x4 and 6x6x3 voxels for this model), and to consider volumes with weights above 1 gram. In addition, rather than averaging the individual SAR values in each of these volumes (since significant portions are likely to be in air because of the irregular shape of the body), it is better to obtain the 1-gram averaged SAR by dividing the total power absorbed in the volume by the total weight of that volume. When a result has been obtained, it is further necessary to carefully scrutinize that volume, and also neighboring volumes, to be certain that the volume is inside the body as much as possible, and that the amount of external air included in the volume is minimized, given the irregular shape of the body [Gandhi, et al., 1996].



Another factor of interest in bioelectromagnetic simulations is the current or current density. The vertical current density is calculated:

$$J_z(i, j, k, t) = \frac{\partial D_z(i, j, k, t)}{\partial t} = \sigma(i, j, k)E_z(i, j, k) + \epsilon_o \epsilon_r(i, j, k) \frac{\partial E_z(i, j, k)}{\partial t} \quad (19)$$

where the derivatives are calculated numerically using (5b). Horizontal current densities are found similarly, and current is found by multiplying by the area. Total current passing through a layer is commonly reported, because this can be compared with experimental results [Gandhi & Chen, 1992 ].

## VII. Computational Issues

### A. Truncated Models

As progressively finer resolution models are used, the amount of required computer memory expands dramatically. For a doubling of resolution (cutting the cell size in half), eight times as much memory is required. In general, this higher resolution is required for higher frequencies, which are known to have minimal penetration into the body. In particular, for cellular telephones, the distal side of the head is almost completely shielded from the telephone. It is therefore possible to reduce the problem size to half or less of the original problem size by truncating the model. This is done with an efficient truncation scheme [Lazzi & Gandhi; Gandhi, et al., 1996]. Because of the minuscule coupling of the far side of the head to the telephone, a second, identical source (telephone) can be placed on the opposite side of the head, leaving the problem unaltered, provided that this second telephone is devoid of RF power (unfed). This model of the two sources, one fed and the other unfed, can be modeled using superposition of two simulations. The first (even) simulation models both sources as positively fed, and the second (odd) simulation models both sources fed, but with the first positively fed, and the second negatively fed. When the two simulations are superimposed, the first source is represented as positively fed, and for the second source, the positive and negative feeds cancel out, and the source is unfed.

The even simulation, which models both phones as positively fed, can be reduced in size by placing a perfect magnetic conductor in the center of the simulation. The odd simulation, which models one phone as positively fed and the other as negatively fed, can be reduced in size by placing a perfect electric conductor in the center of the simulation. Thus, both the even and odd simulation are half as large as originally modeled, so the memory requirement to run them is half of the original problem. In addition, if the power deposition from a single (fed) telephone reaches less than half way into the head, say less than 1/3 of the way into the head, the problem size can be reduced even further. Instead of placing the magnetic and electric conductors in the center of the problem, they are placed 1/3 of the way through the head. To check the validity of this approach, several test cases, including spheres, layered spheres, etc. were considered for an assumed

radiation frequency of 1900 MHz. Excellent agreements were obtained for the SAR distributions from the full, half, and 1/3 models.

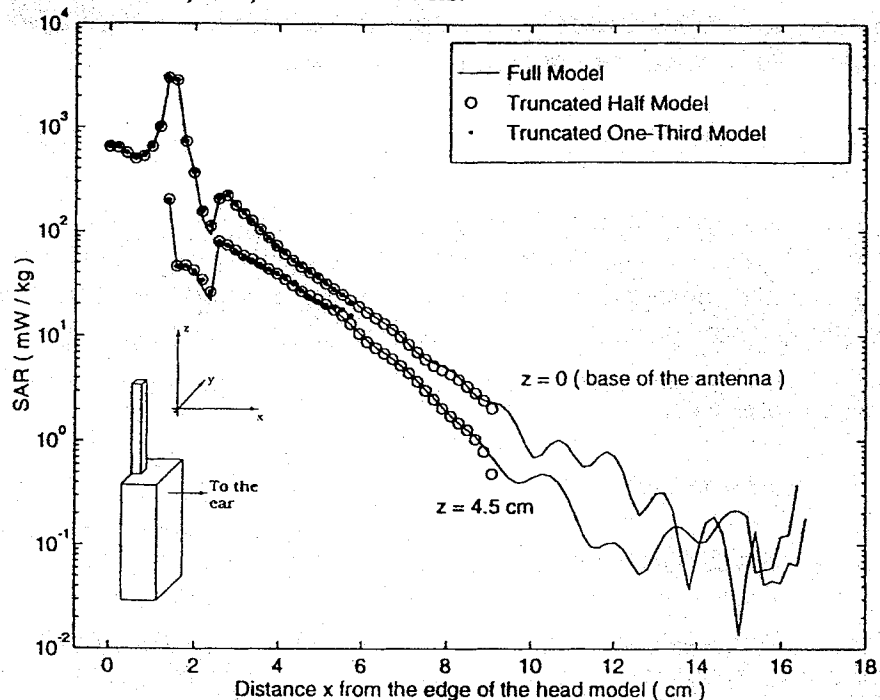


Figure 7 [Gandhi, et al., 1996] shows the SAR distributions obtained for an MRI-based model of the human head for which a quarter-wave monopole over a box is placed against the left ear. The SAR distributions are shown for the whole model, the truncated half model, and the truncated 1/3 model in the plane containing the base of the antenna, and  $z=4.5$  cm above this plane. Minimal error is observed.

The steps to run this truncation method are:

- 1) Pick a plane of symmetry. This is generally chosen to be beyond the penetration of the fields, but can actually be within the field region itself, if errors near this symmetry plane can be tolerated.
- 2) Even simulation: Place a perfect magnetic conductor at the symmetry plane. This is programmed by setting the tangential magnetic fields = 0 on the symmetry plane. Run an FDTD simulation and store the complex values of all fields of interest from this simulation.
- 3) Odd simulation: Place a perfect electric conductor at the symmetry plane. This is programmed by setting the tangential electric fields = 0 on the symmetry plane. Run an FDTD simulation and store the complex of all fields of interest from this simulation.
- 4) Superposition: Add the stored complex values of all fields of interest.

Note: If the only data of interest is in the high field region near the source, either the even or odd simulation alone is generally sufficient. The superposition is required to improve accuracy near the truncation boundary.

## B. Convolution Method

The simple convolution technique is very useful in FDTD and (FD)<sup>2</sup>TD simulations [Chen, et al., 1994]. To apply this technique, the impulse response of the man model is calculated using the complete simulation method, and is stored for later use. When the response of the body to a specific waveform is desired, the impulse response is convolved with the desired waveform to obtain the response of the body to that waveform. This convolution requires far less computational effort than rerunning the complete simulation with the new waveform. These are the steps for the convolution method:

**1a)** Choose an incident impulse waveform  $I_{inc}(t)$  which has a frequency spectrum  $\mathfrak{I}(I_{inc}(t))$  which contains all of the frequency components of interest. An ideal incident impulse is a rectangle function:

$$I_{inc}(t) = \begin{cases} 1 & \text{for } 0 \leq t \leq 5\Delta t \\ 0 & \text{for } t > 5\Delta t \end{cases} \quad (20)$$

which has the frequency spectrum  $\mathfrak{I}(I_{inc}(t)) = 1$  for all frequencies. The frequencies in this pulse which are above the limit of the FDTD grid are dispersed. They do not propagate, and they do not cause aliasing errors in the FDTD simulation, as discussed in section II.

Alternatively:

**1b)** Use a series of continuous sine waves (CW) at each frequency of interest as the incident waveform,  $I_{inc}(t)$ . Combine their Fourier Transforms to find  $\mathfrak{I}(I_{inc}(t))$ .

**2a)** Run the (FD)<sup>2</sup>TD simulation using the incident impulse waveform  $I_{inc}(t)$  as the source function. The (FD)<sup>2</sup>TD method is needed to properly model the frequency dispersion of the tissues over a broad band. Store impulse response of the simulation,  $I_{res}(t)$ . This may be the field component(s) at a given location, the current, power absorbed, or any other value which can be measured as a function of time. Calculate the frequency spectrum of the impulse response,  $\mathfrak{I}(I_{res}(t))$ .

Alternatively:

**2b)** Run the FDTD simulation using single-frequency simulations at each frequency in the band of interest with appropriate tissue properties at each frequency. Superimpose them to obtain  $\mathfrak{I}(I_{res}(t))$ .

**3)** Specify the desired incident waveform  $I_{des}(t)$  and calculate its frequency spectrum,  $\mathfrak{I}(I_{des}(t))$ .

**4)** Find the frequency response of the simulation to the desired waveform:

$$\mathfrak{I}(I_{des\_res}(t)) = \frac{\mathfrak{I}(I_{des}(t))\mathfrak{I}(I_{res}(t))}{\mathfrak{I}(I_{inc}(t))} \quad (21)$$

and find the time domain response of the simulation to the desired waveform:

$$I_{des\_res}(t) = \mathfrak{I}^{-1} \left[ \frac{\mathfrak{I}(I_{des}(t))\mathfrak{I}(I_{res}(t))}{\mathfrak{I}(I_{inc}(t))} \right] \quad (22)$$

## VIII. Examples of Applications

### A. Low Frequency (below 1 MHz)

The biggest limitation of FDTD for low frequency simulations has been that for typical resolutions each cycle has a huge number of time steps, and it is prohibitive to run even a single cycle. For 1mm resolution, for instance, using  $\Delta t = \Delta x / (2c)$  a 60 Hz wave has  $10^{10}$  time steps. This problem was first overcome by [Gandhi & Chen, 1992] using the method of frequency scaling [Guy, et al., 1982]. Frequency scaling observes that in a quasi-static simulation, the simulation can be run at a slightly higher frequency ( $f'$  still in the quasi-static range) than the actual frequency of interest ( $f$ ), and the results can be linearly scaled to the lower frequency using

$$\mathbf{E}(f) = \frac{f}{f'} \mathbf{E}'(f') \quad (23)$$

The simulation is run using the tissue properties at frequency  $f$ , so that no scaling of the tissue properties is required. In [Gandhi & Chen, 1992] the FDTD frequency  $f' = 10$  MHz was used, and scaled to  $f = 60$  Hz. A single cycle (4580 time steps) of the 10 MHz wave was used with peak detection to find the magnitudes of the fields and calculate the total vertical current passing through each layer for comparison with measured values [DiPlacido, et al.], as shown in Figure 8 [Gandhi & Chen, 1992].

A more modern method of obtaining the magnitudes of the fields is to use the method described in (17). For low frequency simulations, the simulation is generally observed to converge in far less than a single cycle (because the body is miniscule compared to a wavelength), and the magnitude can be found by running the simulation only until convergence is reached (a small fraction of a cycle), and using the method in (17) to calculate the magnitudes. There can still be difficulties with numerical roundoff errors in the calculation of the magnitudes, because the waveform is radically oversampled. Frequency scaling significantly reduces the roundoff errors, by reducing the sampling of the waveform. Using a 10 MHz waveform instead of a 60 Hz waveform, for instance, gives a sampling of 60,000 time steps per cycle rather than  $10^{10}$  time steps per cycle. An additional reduction in roundoff error can be obtained by choosing the two time steps,  $t_1$  and  $t_2$  reasonably far apart. The least error will occur when the time steps are a quarter wavelength apart, but far less is sufficient. Using 100 time steps between  $t_1$  and  $t_2$  gives roundoff errors on the order of  $10^{-6}$  at 10 MHz, and this is generally more than sufficient for dosimetric calculations. An additional reason to use frequency scaling for

low frequency simulations is that the field values inside the body decrease linearly with frequency following (23), so that at low frequencies, the fields penetrating into the body are substantially lower than on the outside of the body. This causes significant roundoff errors in the FDTD calculations, which can again be avoided by using frequency scaling.

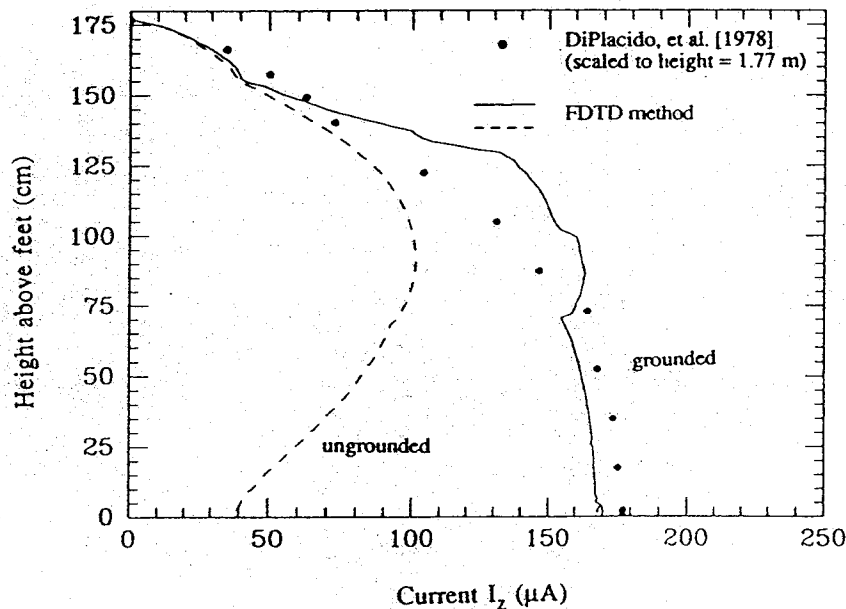


Figure 8: Calculated layer currents for saline-filled grounded and ungrounded human models exposed to a vertical 10 kV/m, 60 Hz electric field. For the FDTD techniques,  $H_{inc} = 26.5$  A/m oriented from side-to-side of the body has also been included. Measured values are given in [DiPlacido, et al.], calculated values given in [Gandhi & Chen, 1992]

Another issue in low-frequency simulations is the absorbing boundary conditions. The PML boundary condition has been shown to be effective (errors less than 5%) at low frequencies, if the number of time steps is minimized. Mur boundary conditions, perhaps surprisingly, do not completely break down but are slightly less accurate than the PML conditions [De Moerloose, et al.].

### B. Mid-Frequency (1 MHz - 1 GHz)

The FDTD method has been applied to a myriad of mid-frequency simulations including calculation of SARs and induced currents in the human body for plane wave exposures [Gandhi, et al., 1992], exposure to the leakage fields of parallel-plate dielectric heaters [Chen & Gandhi, 1991a], exposure to EMP [Chen & Gandhi, 1991b], annular phased arrays of aperture, dipole, and insulated antennas for hyperthermia [Chen & Gandhi, 1992], coupling of the cellular telephones to the head [Gandhi, et al., 1996; Jensen & Rahmat-Samii; Dimbylow & Mann; Luebbers, et al., 1992; Okoniewski & Stuchly; Watanabe, et al.], and exposure to RF magnetic fields in magnetic resonance imaging

(MRI) machines [Gandhi, et al., 1994]. Tissue properties and human models are well-established in this frequency band, and the FDTD method is a well-accepted simulation method in this range.

Simulations of the coupling of cellular telephones to the head has shown that the head absorbs 40-50% of the power radiated from an isotropic antenna such as is commonly used on cellular phones [Gandhi, et al., 1996 ], and that consequently the head significantly alters the radiation patterns from these phones [Jensen & Rahmat-Samii; Okoniewski & Stuchly ] and also the matching characteristics of the antenna. The cellular telephones are generally modeled as a metal box covered by plastic. The size of this box has been shown to influence the radiated fields and SAR distribution patterns [Gandhi, et al., 1996]. In addition, the plastic covering the box and antenna also affects these parameters. Since the plastic is generally thinner than the resolution of the FDTD grid, an effective dielectric constant is used in this cell to model the plastic [Gandhi, et al., 1996]. This effective dielectric constant,  $K_e$ , is derived by noting that the electric fields close to a metallic surface such as that of a handset are primarily normal to the metal, and only a part of the FDTD-cell width is actually filled with the dielectric material. The required continuity of the normal component of  $\mathbf{D}=\epsilon\mathbf{E}$  with the outer region can be used to obtain  $K_e$ . This gives an equation for  $K_e$  in an FDTD cell of size  $\delta$  which is somewhat lower than the dielectric constant of the plastic,  $\epsilon_r$ , of thickness  $w$  (generally about 1mm)

$$K_e = \frac{\delta / \epsilon_r}{[\epsilon_r (\delta - w) + w]} \quad (24)$$

Here  $\delta$  is the dimension of the FDTD cell, which is  $\delta_x, \delta_y, \delta_z$  depending on which surface of the metal handset or antenna is being considered.

Elements of cellular telephone simulations which have been found to significantly affect the accuracy of the simulation include the size of the metal box of the telephone and the dielectric properties used for the head [Gandhi, et al., 1996]. It has been shown that several different head models (with ears removed) can provide similar results, although homogeneous models have been found to significantly overestimate the 1-gram SAR value (by roughly 30%) [Gandhi, et al., 1996; Hombach, et al.]. Although [Hombach, et al.] did not consider the effect of ear shape, it is likely that the shape of the ear (pressed against the head or not pressed against the head) does affect the local SAR distribution. Two of the most significant parameters affecting the power deposition in the head from the cellular telephone is the nature of the antenna (length, shape, etc.) and how close it is to the head. For accurate modeling, it is essential to properly represent the length of the antenna, the exact configuration of the feedpoint (especially if any metal parts such as those used to hold the antenna protrude above the top of the box), and the exact location of the antenna on the top of the box. This can be done with engineering drawings or xrays of the actual phone. For accuracy, it is a good idea to model the telephone without the head first, and compare to a known measured value such as radiation pattern or near-field measurements without the head, to ensure that the model of the telephone and antenna is accurate. Once the telephone model is verified, there is still the question of how to position the telephone relative to the head. This has been done several different ways in

the literature. One school of thought is to find the absolute worst position the phone could be held in, such as directly in front of and nearly touching the eye. Another school of thought is to position it in approximately the position it would be used, but without the ear, as the ear significantly complicates both measurements and interpretation of the measurements [Gandhi, et al., 1996]. Still another school of thought is to attempt the most realistic placement for ordinary operation of the phone, including the effect of the ear [Lazzi & Gandhi, 1996]. In this case, the ear is compressed as it generally is when people press the phone against their ear. Care is taken to line up the listening microphone with the ear canal, as this is observed to be the position where the phone is generally used. The effect of tilting the telephone towards the mouth, in the most realistic position, has also been examined [Lazzi & Gandhi, 1996]. In this case, the telephone is modeled on the vertical FDTD grid, and the head is tipped, to prevent errors due to stair-case modeling of the metal phone parts.

As an example of the effect of these parameters, Table 1 shows a comparison of several different orientations of the head for a 2.76 x 5.73 x 15.5 cm telephone at 835 MHz, covered with 1 mm of plastic (modeled as one cell thick using (24)), with a  $\lambda/4$  antenna, also coated with plastic. The phone model is held against the Utah model of the human head, and the simulation has an overall resolution of 1.974 x 1.974 x 3mm. Three values are shown, one for the phone held vertical to the head, touching the ear, which is pressed against the head. The second model has the phone tilted towards the mouth, but not pressed against the cheek, and the third model has the phone tilted towards the mouth and pressed against the cheek. As the phone is tilted towards the mouth, the antenna is effectively tilted away from the head, thus lowering the localized values very near the antenna, and consequently the 1-gram SAR value. This effect is most notable for physically long antennas. For the shorter antenna used at 1900 MHz, the 1-gram SAR is not lowered significantly as the phone is tilted. This is because the antenna remains very near the head, despite being tilted

Table 1: Comparison of the 1-gram SARs for a cellular telephones next to the head as a function of phone position [Lazzi and Gandhi, 1996]

Frequency (MHz)	Vertical Head Model	Tilted 30 degrees head Model	Tilted 30 degrees head model with additional rotation of 9 degrees
835	2.93 W/kg	2.44 W/kg	2.31 W/kg
1900	1.11 W/kg	1.08 W/kg	1.20 W/kg

### C. High Frequency (above 1 GHz)

The use of the FDTD method for high frequency simulations is limited only by the resolution of the grid and the ability of the computer to analyze the very large models which result from small grid resolutions. Fortunately, at high frequencies, the power deposition is highly superficial, so methods such as truncating the model [Lazzi & Gandhi, 1996] are highly effective. This method has been used for cellular telephones working at 6 GHz [Gandhi and Chen, 1995]

### D. Broad-Band

Since the properties of biological tissue are significantly frequency dispersive, one of two methods must be used to predict broad-band effects. Either the convolution method must be used, where individual FDTD simulations are run at every frequency of interest (where tissue properties can be precisely prescribed), as described in section II, or the  $(FD)^2TD$  method should be used as described in section III. The convolution method is very cumbersome if a large number of frequencies are of interest. The relative accuracy of the two methods depends on the accuracy of the Debye equation (13) fits to the measured tissue properties. If the match is perfect, the two methods provide identical accuracy. If the match has some error, the error observed in the  $(FD)^2TD$  simulation is the same as would have occurred if the FDTD simulation had been run with that error in the tissue properties. In general, truly broad-band simulations have such a large number of frequencies in the pulse that the  $(FD)^2TD$  is preferable to multiple FDTD simulations.

As an example, the FDTD and  $(FD)^2TD$  methods were compared for finding the layer-averaged SARs in a 1.31 cm resolution model of the human body over the frequency range from 20 to 915 MHz [J.Y. Chen, et al., 1994]. Figure 9 shows the layer-averaged RF current at 40, 150, and 350 MHz for this simulation.

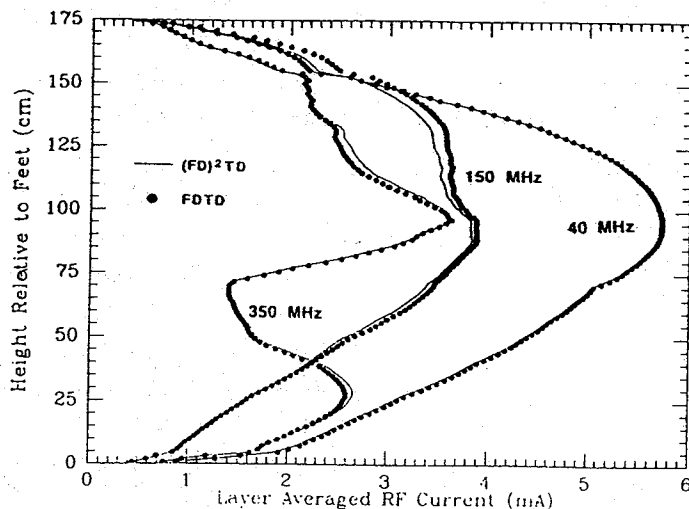


Figure 9: Layer-averaged RF currents in the human model comparing the accuracy of the FDTD and  $(FD)^2TD$  solutions. Tissue properties are modeled with second-order Debye equations.



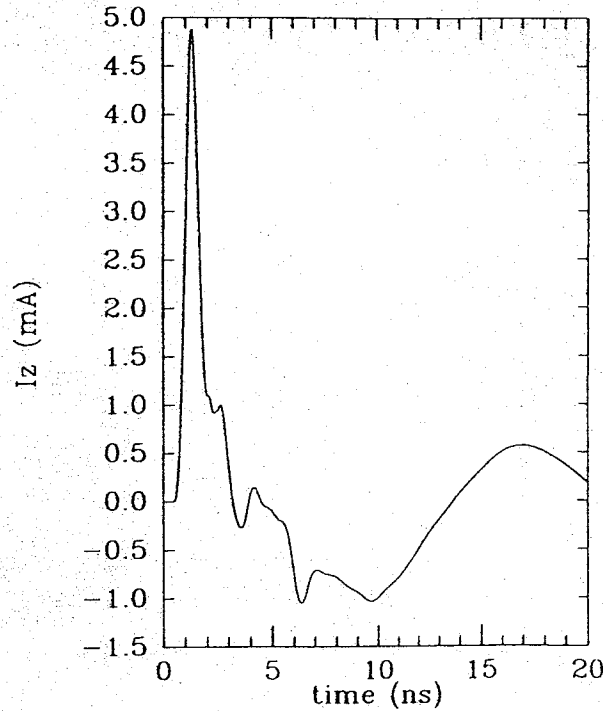


Figure 10: Time-domain currents through the heart, simulated using the  $(FD)^2TD$  method.

The results of the  $(FD)^2TD$  simulation are shown in Figure 10 in the time-domain for a raised-cosine pulse which has a bandwidth from 0 to 915 MHz. The layer-averaged current is shown for the layers of the eyes and the ankles. This broad-band time-domain simulation would have been prohibitively cumbersome to obtain without the  $(FD)^2TD$  method because of the large number of frequencies in this pulse.

## V. Conclusions

The FDTD method has proven to be one of the most flexible, efficient, and applicable methods for numerical calculations of electromagnetic interaction with the body from the quasi-static to near-optic range. It lends itself particularly well to modeling the heterogeneities of the human body in millimeter resolution, and to modeling a wide variety of electromagnetic sources in the far field or very near the body. In addition to the basic efficiency of the algorithm, numerous additions to the method make the application of this method even more efficient for particular applications. The FDTD algorithm is efficiently programmed for either serial or parallel machines, and is found to scale very near linearly as the number of processors is increased. Methods to reduce the model size such as grid truncation have been shown to be highly effective. Signal processing techniques can be optimized for this method, and a frequency-dependent FDTD method provides data for

broad-band simulations. The flexibility and efficiency of this simple algorithm have made it the popular electromagnetics simulation method that it is.

## REFERENCES

ANSI/IEEE C95.1-1992, "American National Standard --- safety levels with respect to exposure to radio frequency electromagnetic fields, 3 kHz to 300 GHz," published by the Institute of Electrical and Electronic Engineers, Inc., 345 East 47<sup>th</sup> Street, New York, New York, 10017

Bi, Z., Y. Shen, K. Wu, J. Litva, "Fast finite-difference time-domain analysis of resonators using digital filtering and spectrum estimation techniques," *IEEE Trans. Microwave Theory and Tech.*, pp. 1611-1619, 1992

Borup, D.T., D.M. Sullivan, O.P. Gandhi, "Comparison of the FFT conjugate gradient method and the FDTD method for the 2D absorption problem," *IEEE Trans. Microwave Theory and Tech.*, pp. 383-395, 1987

Bui, M.D., S.S. Stuchly, G.I. Costache, "Propagation of transients in dispersive dielectric media," *IEEE Trans. Microwave Theory and Tech.*, Vol. MTT-39, pp. 1165-1172, July 1991

Chen, J.Y., O.P. Gandhi, D.L. Conover, "SAR and induced current distributions for operator exposure to RF dielectric sealers," *IEEE Trans. Electromagnetic Compatibility*, 33(3), pp. 252-161, 1991

Chen, J.Y., O.P. Gandhi, "Currents induced in an anatomically based model of a human for exposure to vertically polarized electromagnetic pulses," *IEEE Trans. Microwave Theory and Techniques*, 39(1), pp. 31-39, 1991

Chen, J.Y., O.P. Gandhi, "Numerical simulation of annular-phased arrays of dipoles for hyperthermia of deep-seated tumors," *IEEE Trans. Biomed. Eng.*, 39(3), pp. 209-216, 1992

Davis, C.C., G. A. Katona, L.S. Taylor, "Dielectric measurement of tissues in the mammalian head at cellular telephone frequencies," 18<sup>th</sup> Annual meeting of the Bioelectromagnetics Society, Victoria, B.C., June 9-14, 1996

De Moerloose, J., T.W. Dawson, M.A. Stuchly, "Application of FDTD to quasi-static field analysis," personal communication

Deno, D.W. "Currents induced in the human body by high voltage transmission line electric field - measurement and calculation of distribution and dose," *IEEE Trans. Power Apparatus and Systems*, Vol. PAS-96 (5), pp. 1517-1527, Sept./Oct. 1977

- Dhondt, G., L. Martens, "A canonical case with an analytical solution for the comparison of electromagnetic field solvers," Proceedings of the COST 244 meeting on Reference Models for Bioelectromagnetic Test of Mobile Communication Systems, D. Suminic, Editor
- Dimbylow, P.J., and S. M. Mann, "SAR Calculations in an Anatomically Based Realistic Model of the Head for Mobile Communication Transceivers at 900 MHz and 1.8 GHz," *Physics in Medicine and Biology*, Vol. 39, pp. 1537-1553, 1994
- Dimbylow, P.J., "The development of realistic voxel phantoms for electromagnetic field dosimetry," *Voxel Phantom Development: Proceedings of an International Workshop held at the National Radiological Protection Board, Chilton, UK, July 6-7, 1995*, Peter J. Dimbylow, editor
- DiPlacido, J., C.H. Chih, B.J. Ware, "Analysis of the proximity effects in electric field measurements," *IEEE Trans. Power Apparatus Systems*, Vol. 97, pp. 2167-2177, 1978
- Durney, C.H., C.C. Johnson, P.W. Barber, H. Massoudi, M.F. Iskander, J.L. Lords, D.K. Ryser, S.J. Allen, J.C. Mitchell, *Radiofrequency Radiation Dosimetry Handbook*, 2<sup>nd</sup> ed., USAF School of Medicine, Brooks AFB, TX, 1978
- FCC 96-326, "Guidelines for evaluating the environmental effects of radiofrequency radiation," Aug. 1, 1996, available from the Federal Communications Commission, Washington, D.C. 20554
- Foster, K.R., H. Schwan, Table 5, *Critical Reviews in Biomedical Engineering*, Vol. 17(1), pp. 25-104, 1989
- Furse, C.M. "Use of the FDTD method for broad band calculations of electromagnetic scattering and absorption from large, heterogeneous scatterers," PhD Dissertation, University of Utah, 1994
- Furse, C.M., J.-Y. Chen, O.P. Gandhi, "The use of the frequency-dependent finite-difference time-domain method for induced current and SAR calculations for a heterogeneous model of the human body," *IEEE Trans. Electromagnetic Compatibility*, 36(2), 128-133, 1994
- Furse, C.M., S.P. Mathur, O.P. Gandhi, "Some improvements to the FDTD method for calculating radar cross section of a perfectly conducting target," *IEEE Trans. Microwave Theory and Tech.*, Vol. 38, pp. 919-927, 1990
- Furse, C.M., O.P. Gandhi, "Calculation of Electric Fields and Currents Induced in a mm-Resolution Human Model with a Novel Time-to-Frequency Domain Conversion," IEEE Antennas and Propagation Society Conference, Baltimore, MD, July 21-25, 1996

Gabriel, C., "Compilation of the dielectric properties of body tissues at RF and microwave frequencies," Final Report AL/OE-TR-1996-0037 submitted to Occupational and Environmental Health Directorate, RFR Division, 2503 Gillingham Dr., Brooks AFB, TX, June 1996

Gandhi, O.P., J.Y. Chen, "Numerical dosimetry at power-line frequencies using anatomically-based models," *Bioelectromagnetics Supplement I*, pp. 43-60, 1992

Gandhi, O.P., Y.G. Gu, J.Y. Chen, H.I. Bassen, "Specific absorption rates and induced current distributions in an anatomically based human model for plane-wave exposures," *Health Physics*, 63(3), pp. 281-290, 1992a

Gandhi, O.P., B.Q. Gao, J.Y. Chen, "A frequency-dependent finite-difference time-domain formulation for induced current calculations in human beings," *Bioelectromagnetics*, Vol.3, pp. 47-71, 1992b

Gandhi, O.P., B.Q. Gao, J.Y. Chen, "A frequency-dependent finite-difference time-domain formulation for general dispersive media," *IEEE Trans. Microwave Theory and Tech* 41(4), pp. 658-665, 1993a

Gandhi, O.P., C.M. Furse, "Currents induced in the human body for exposure to ultrawideband electromagnetic pulses," Final Report AI-TR-1992-0156 to Occupational and Environmental Health Directorate, RFR Division, Brooks AFB, TX, May 1993

Gandhi, O.P., S.B. Chen, X.Yuan, J.Y. Chen, "Dosimetry for time-varying magnetic fields in MR Imaging," p. 16, *Abstracts of Sixteenth Annual Meeting of the Bioelectromagnetics Society*, Copenhagen, Denmark, June 12-17, 1994

Gandhi, O.P. "Some experimental methods for dosimetry: Extremely low frequencies to microwave frequencies," *Radio Science*, 30(1), 161-177, 1995

Gandhi, O.P., C.M. Furse, "Millimeter-resolution MRI-based models of the human body for electromagnetic dosimetry from ELF to microwave frequencies," *Voxel Phantom Development: Proceedings of an International Workshop held at the National Radiological Protection Board*, Chilton, UK, July 6-7, 1995, Peter J. Dimbylow, editor

Gandhi, O.P., J.Y. Chen, "Electromagnetic absorption in the human head from experimental 6 GHz handheld transceivers," *IEEE Trans. Electromagnetic Compatibility*, 37(11), 547-558, 1995

Gandhi, O.P., J.Y. Chen, "Electromagnetic absorption in the human head from experimental 6 GHz hand-held transceivers," *IEEE Trans. Electromagnetic Compatibility*, Vol. 37, pp. 547-558, 1995

Gandhi, O.P., G.Lazzi, C.M. Furse, "Electromagnetic Absorption in the human head and neck for mobile telephones at 835 and 1900 MHz," *IEEE Trans. Microwave Theory and Tech.*, 44(10), Oct. 1996

Gao, B.-Q., O.P. Gandhi, "An expanding grid algorithm for the FDTD method," *IEEE Trans. Electromagnetic Compatibility*, pp. 277-283, 1992

Geddes, L.A., L.E. Baker, "The specific resistance of biological material – a compendium of data for the biomedical engineer and physiologist," *Med. & Biol. Engng.*, Vol. 5, pp. 271-293, Pergamon Press, 1967

Guy, A.W., S. Davidow, G.Y. Yang, C.K. Chou, "Determination of electric current distributions in animals and humans exposed to a uniform 60-Hz high-intensity electric field," *Bioelectromagnetics*, Vol.3, pp. 47-71, 1982

Holland, R., L. Simpson, K.S. Kunz, "Finite-difference analysis of EMP coupling to lossy dielectric structures," *IEEE Trans. Electromagnetic Compatibility*, pp. 203-209, 1980

Hombach, V., K.Meier, M. Burkhardt, E. Kuhn, N.Kuster, "The dependence of EM energy absorption upon human head modeling at 900 MHz," *IEEE Trans. Microwave Theory and Tech.*, 44(10), pp. 1865-1873, 1996

Jensen, M.A., Y. Rahmat-Samii, "EM interaction in handset antennas and a human in personal communications," *Proc. IEEE*, 83, pp.7-17, 1995

Joseph, R.M., S.C. Hagness, A. Taflove, "Direct time integration of Maxwell's equations in linear dispersive media with absorption for scattering and propagation of femtosecond electromagnetic pulses," *Optics Letters*, Vol 16(18), pp. 1412-1414, Sept. 1991

Kunz, K.S., K.M. Lee, "A three-dimensional finite-difference solution of the external response of an aircraft to a complex transient EM environment: Part II—Comparison of predictions and measurements," *IEEE Trans. Electromagnetic Compatibility*, pp. 333-341, 1978

Kunz, K.S., R.J. Luebbers, *The Finite-Difference Time-Domain Method in Electromagnetics*, CRC Press, Boca Raton, FL, 1993

Lazzi, G., O.P. Gandhi, "Realistically titled and truncated anatomically based models of the human head for dosimetry of mobile telephones," to be published in *IEEE Trans. Electromagnetic Compatibility*

Lee, C.F., R.T. Shin, J.A. Kong, "Application of FD-TD technique to dispersive materials," *PIERS Proceedings*, 1991

- Lin, J.C., O.P. Gandhi, "Computational methods for predicting field intensity," *CRC Handbook Biological Effects Electromagnetic Fields*, 2<sup>nd</sup> ed., C.Polk and E. Postow, Eds., CRC Press, Boca Raton, FL, ch. 9, pp. 335-339, 1995
- Luebbers, R., L.Chen, T. Uno, S. Adachi, "FDTD Calculation of Radiation Patterns, Impedance and Gain for a Monopole Antenna on a Conducting Box," *IEEE Trans. Antennas and Propagation*, Vol. 40, pp. 1577-1582, 1992
- Luebbers, R., F. Hunsberger, K. Kunz, "A frequency-dependent finite-difference time-domain formulation for transient propagation in plasma," *IEEE Trans. Antennas and Propagation*, pp. 29-34, 1991
- Luebbers, R., F. Hunsberger, K. Kunz, "FDTD for Nth order dispersive media," submitted to *IEEE Trans. Antennas and Propagation*, 1992
- Luebbers, R.J., F.P.Hunsberger, K.S. Kunz, R.B. Standler, M. Schneider, "A frequency-dependent finite-difference time-domain formulation for dispersive materials," *IEEE Trans. Electromagnetic Compatibility*, Vol. EMC-22, pp. 222-227, Aug. 1990
- Luebbers, R., L.Chen, T. Uno, S. Adachi, "FDTD calculation of radiation patterns, impedance, and gain for a monopole antenna on a conducting box," *IEEE Trans. Antennas and Propagation*, Vol. 40, pp. 1577-1582, 1992
- Okoniewski, Michal, M.A. Stuchly, "A study of the handset antenna and human body interaction," *IEEE Trans. Microwave Theory and Tech.*, 44(10), pp. 1855-1864, 1996
- Olley, P., P.S. Excell, "Classification of high resolution voxel image of a human head," *Voxel Phantom Development: Proceedings of an International Workshop held at the National Radiological Protection Board*, Chilton, UK, July 6-7, 1995, Peter J. Dimbylow, editor
- National Library of Medicine, Visible Man Project, MRI scans, CT scans, and photographs available on CD through Research Systems, Inc., 2995 Wilderness Place, Boulder, CO 80301
- Oristaglio, M.L., G.W. Hohmann, "Diffusion of electromagnetic fields into a two-dimensional earth: a finite-difference approach," *Geophysics*, pp. 870-894, 1984
- Rush, S., J.A. Abildskov, R. McFee, "Resistivity of body tissues at low frequencies," *Circ. Research*, Vol. XII, pp. 40-50, 1963
- Snyder, W.S., M.J. Cook, E.S. Nasset, L.R. Karhausen, G.P. Howells, I.H. Tipton, Report of the Task Group on Reference Man, Pergamon Press, 1995

Stuchly, M.A., S.S. Stuchly, "Dielectric properties of biological substances – tabulated," *J. Microwave Power*, 15(1), pp. 19-26, 1980

Stuchly, M.A., K. Caputa, A. van Wensen, A. El-Sayed, "Models of human and animal bodies in electromagnetics," *Voxel Phantom Development: Proceedings of an International Workshop held at the National Radiological Protection Board, Chilton, UK, July 6-7, 1995*, Peter J. Dimbylow, editor

Sullivan, D.M., "Use of the FDTD method in electromagnetic dosimetry," Ph.D. Dissertation, Chapter 1, University of Utah, 1987

Sullivan, D.M., "A frequency-dependent FDTD method for biological applications," *IEEE Trans. Microwave Theory and Tech.*, Vol. MTT-40, pp. 532-539, March 1992

Taflove, A., *Computational Electrodynamics: The Finite-Difference Time-Domain Method*, Artech House, Dedham, MA, 1995

Taflove, A., M. Brodwin, "Numerical solution of steady-state electromagnetic scattering problems using the time-dependent Maxwell's equations," *IEEE Trans. Microwave Theory and Tech.*, pp. 623-630, 1975

Taflove, A., K.R. Umashankar, T.G. Jurgens, "Validation of the FDTD modeling of the radar cross section of three-dimensional structures spanning up to nine wavelengths," *IEEE Trans. Antennas and Propagation*, pp. 662-666, 1985

Umashankar, K., A. Taflove, "A novel method to analyze electromagnetic scattering of complex objects," *IEEE Trans. Electromagnetic Compatibility*, pp. 397-424, Nov. 1982

Watanabe, S., M. Taki, T. Nojima, O. Fujiwara, "Characteristics of the SAR distributions in a head exposed to electromagnetic fields radiated by a hand-held portable radio," *IEEE Trans. Microwave Theory and Tech.*, 44(10), pp. 1874-1883, 1996

Yee, K.S., "Numerical solution of initial boundary problems involving Maxwell's equations in isotropic media," *IEEE Trans. Antennas and Propagation*, Vol. 41, pp. 302, 1966